Check for updates

ARTICLE

Commensal gut bacterium critically regulates alveolar bone homeostasis

Jessica D. Hathaway-Schrader [1,2,3], Matthew D. Carson[1,2,3], Joy E. Gerasco[1], Amy J. Warner [1,2,3], Brooks A. Swanson[1,2,3], J. Ignacio Aguirre[4], Caroline Westwater [1,5], Bei Liu[6] and Chad M. Novince[1,2,3 ✉]

The alveolar bone is a unique osseous tissue due to the presence of the teeth and the proximity of commensal oral microbes. Commensal microbe effects on alveolar bone homeostasis have been attributed to the oral microbiota, yet the impact of commensal gut microbes is unknown. Study purpose was to elucidate whether commensal gut microbes regulate osteoimmune mechanisms and skeletal homeostasis in alveolar bone. Male C57BL/6T germfree (GF) littermate mice were maintained as GF or monoassociated with segmented filamentous bacteria (SFB), a commensal gut bacterium. SFB has been shown to elicit broad immune response effects, including the induction of T_H17/IL17A immunity, which impacts the development and homeostasis of host tissues. SFB colonized the gut, but not oral cavity, and increased IL17A levels in the ileum and serum. SFB had catabolic effects on alveolar bone and non-oral skeletal sites, which was attributed to enhanced osteoclastogenesis. The alveolar bone marrow of SFB vs. GF mice had increased dendritic cells, activated helper T-cells, T_H1 cells, T_H17 cells, and upregulated *Tnf*. Primary osteoblast cultures from SFB and GF mice were stimulated with vehicle-control, IL17A, or TNF to elucidate osteoblast-derived signaling factors contributing to the pro-osteoclastic phenotype in SFB mice. Treatment of RAW264.7 osteoclastic cells with supernatants from vehicle-stimulated SFB vs. GF osteoblasts recapitulated the osteoclast phenotype found in vivo. Supernatants from TNF-stimulated osteoblasts normalized RAW264.7 osteoclast endpoints across SFB and GF cultures, which was dependent on the induction of CXCL1 and CCL2. This report reveals that commensal gut microbes have the capacity to regulate osteoimmune processes in alveolar bone. Outcomes from this investigation challenge the current paradigm that alveolar bone health and homeostasis is strictly regulated by oral microbes.

INTRODUCTION

Commensal microbes colonize the host to establish a relationship in which one derives benefit without obvious harm or benefit to the other[1]. Collections of microbes colonize distinct anatomical sites to form microbiota communities (i.e., oral microbiota, gut microbiota, skin microbiota)[1–3]. The commensal microbiota critically regulates host immunity[3–6], which has indirect effects on the physiology and homeostasis of host tissues[6–10]. Commensal microbiota effects on host immunity have recently been shown to impact osteoimmunology[11–14], which is the process by which immune cells regulate bone cells[15]. Commensal microbiota regulation of osteoimmune mechanisms critically influences the turnover and homeostasis of the skeleton in both health and disease[11–15].

Alveolar bone formation and homeostasis are dependent on the eruption and maintenance of the teeth. The teeth are a mineralized transmucosal organ that is vigorously colonized by oral microbes. The alveolar bone is distinct from all other bone tissues, due to the teeth acting as a scaffold for oral microbe biofilms that form in close proximity to alveolar bone[16,17].

Commensal oral microbes elicit local immune responses in barrier epithelial and gingival connective tissues, which modulate osteoimmune signaling and coupled osteoclast-osteoblast actions at the subjacent alveolar bone[12,17].

Gnotobiology is the science of studying animals with a defined microbiota. Germfree (GF) animals are associated (colonized) with specific microorganisms to elucidate host-microbe interactions. Early investigators monoassociated GF rats with different commensal oral bacteria to delineate that commensal oral microbes critically regulate alveolar bone homeostasis[18–20]. Due to the proximity of the oral microbiota to alveolar bone, current theory supports the notion that alveolar bone homeostasis is strictly regulated by oral microbes[17]. Recognizing that commensal gut microbes modulate systemic immunity[3–6], the purpose of the current report was to delineate whether commensal gut microbes have the capacity to regulate osteoimmune mechanisms and skeletal homeostasis in the alveolar bone complex.

We innovatively utilized the segmented filamentous bacteria (SFB)-monoassociated mouse model, which is devoid of oral microbes, to

[1]Department of Oral Health Sciences, College of Dental Medicine, Medical University of South Carolina, Charleston, SC, USA. [2]Department of Stomatology—Division of Periodontics, College of Dental Medicine, Medical University of South Carolina, Charleston, SC, USA. [3]Department of Pediatrics—Division of Endocrinology, College of Medicine, Medical University of South Carolina, Charleston, SC, USA. [4]Department of Physiological Sciences, College of Veterinary Medicine, University of Florida, Gainesville, FL, USA. [5]Department of Microbiology and Immunology, College of Medicine, Medical University of South Carolina, Charleston, SC, USA. [6]Department of Internal Medicine—Division of Hematology, College of Medicine, The Ohio State University, Columbus, OH, USA. ✉email: novincec@musc.edu

discern whether commensal gut microbes impart osteoimmune response effects in alveolar bone. SFB is a commensal gut bacterium that resides in the gastrointestinal tracts of a wide variety of species, including rodents and humans[21–26]. SFB colonizes the terminal ileum of mice post weaning and maintains its presence in the intestinal tract throughout post-natal development and young adulthood[27–30]. SFB adheres to intestinal epithelial cells to elicit broad innate and adaptive immune response effects, including the induction of T_H17/IL17A immunity[31–38]. SFB promotion of T_H17/IL17A immunity confers protection against pathogenic microbes, both locally in the gut[31,39,40] and at distant anatomic sites[41]. SFB actions on systemic immunity influence host tissue homeostasis at extraintestinal sites, including the skeleton[42–45]. Two recent osteoimmunology reports relied on the presence of SFB in the gut to discern that specific commensal gut microbes regulate osteoimmune processes at non-oral skeletal sites[44,45].

To our knowledge, this is the first known report to employ a gnotobiotic animal model to determine whether commensal gut microbes have the capacity to regulate osteoimmune mechanisms in the alveolar bone complex. In line with prior work which showed that SFB enhanced both IL17A and TNF[45–47], we demonstrated that SFB osteoimmune actions are linked to the induction of IL17A and TNF. Based on the knowledge that IL17A and TNF can promote osteoblasts to secrete pro-osteoclastic factors[48–53], we established an in vitro osteoblast-osteoclast coupling assay targeting IL17A and TNF. This model system provides initial evidence demonstrating that commensal gut microbe immunomodulatory actions influence osteoimmune crosstalk. Notably, this work discerns that commensal gut microbes have the ability to regulate osteoimmune processes and skeletal homeostasis in the alveolar bone complex. Findings from this study challenge the current paradigm that alveolar bone health and homeostasis are strictly regulated by oral microbes.

MATERIALS AND METHODS

Mice
GF C57BL/6T mice were acquired from Taconic Biosciences (Rensselaer, NY), bred, and maintained in sterile isolators at Medical University of South Carolina (MUSC) Gnotobiotic Animal Core. Male GF littermates were maintained as GF or monoassociated with SFB at age 5 weeks. SFB-monoassociated mice were generated as previously described[44]. Animals were euthanized at age 11 weeks and tissues were harvested for analyses. Animal protocols were approved by the MUSC Animal Protocols Review Board and were done in accordance with the National Institutes of Health Guide for Care and Use of Laboratory Animals.

Micro-CT
Femurs and maxillae were fixed in 10% phosphate-buffered-formalin for 24 h at room temperature and then stored in 70% ethanol. Specimens were scanned with Bruker Skyscan 1176 (Bruker, Kontich, Belgium) with the following acquisition parameters: aluminum 0.5 mm filter, rotation step of 0.3°, average of two frames at 4000 × 2612 dpi, X-ray tube potential at 50 kVp, X-ray intensity of 497 μA, 65 ms integration time, and isotropic voxel size of 9 μm³. Calibrated three-dimensional images were reconstructed.

Trabecular bone volume per tissue volume was analyzed in femurs and maxillae via AnalyzePro 12.0 Bone Microarchitecture Analysis software (Analyze Direct, Seattle, WA). For femurs, transverse CT slices were evaluated beginning 450 μm distal to the proximal growth plate and extending 1500 μm distally. A fixed threshold of 250 Hounsfield Units was utilized to discern mineralized tissue. Data are reported in accordance with standardized nomenclature[54], as previously described[13,44,55]. For maxillae, trabecular bone volume per tissue volume analysis was performed in the maxillary 1st molar trifurcation, within a defined volume of interest (VOI). The VOI was created by linearly morphing a cylinder within the trifurcation, excluding the periodontal ligament, lining the mesiobuccal, distobuccal, and lingual roots and the endocortical surface of the buccal and lingual cortical plates. The height of the cylinder was set so that the superior aspect of the cylinder was positioned apical to the fornix of the trifurcation, and the inferior aspect of the cylinder was positioned at the apex of the

distobuccal root. Fixed threshold of 250 Hounsfield units was used to discriminate mineralized tissue.

Reconstructed maxillae images were also used to assess linear alveolar bone loss. Linear alveolar bone loss was assessed at the maxillary first molar using AnalyzePro Analysis software (Analyze Direct, Seattle, WA). Linear alveolar bone loss was evaluated by measuring the linear distance from the cementoenamel junction (CEJ) to the alveolar bone crest (ABC) at the mesiobuccal line angle, distobuccal line angle, and mid-lingual aspect of the maxillary first molar (Supp Fig. 1). The CEJ to ABC linear measurements were performed to evaluate alveolar bone loss. CEJ to ABC linear distance is used both clinically and experimentally to accurately assess alveolar bone loss[16,56]. The maxillary first molar was oriented in the axial plane such that the mid-buccal-lingual aspect of the mesiobuccal and distobuccal roots were aligned to a horizontal plane at 0°. The first molar was oriented in the sagittal plane such that the CEJ at the mesial and distal aspect of the tooth were aligned to a horizontal plane at 0°. Within the axial plane, the coronal height of contour was determined at the mesiobuccal line angle, distobuccal line angle, and mid-lingual aspect of the molar. These landmarks served as the midpoint for carrying out CEJ to ABC linear measurements. The initial measurement was performed at the mid-point, two subsequent measurements were carried out 45 μm and 90 μm mesial to the midpoint, and two additional measurements were performed 45 μm and 90 μm distal to the midpoint.

Histomorphometry
Maxillae and femurs were fixed in 10% phosphate-buffered formalin for 24 h at room temperature. Specimens were then decalcified in 14% EDTA for 3 weeks at room temperature, processed for paraffin embedding, and 5 μm serial sagittal sections were cut using an Accu-Cut SRM 200 Sakura microtome (Sakura Finetek Europe B.V, Zoeterwoude, NL). Serial sagittal sections were cut through the maxillary first molar and distal femur and stained with tartrate-resistant acid phosphatase (TRAP). Maxillae were counterstained with aniline blue. Histomorphometric analysis of osteoclast cellular outcomes was performed in TRAP-stained sections where TRAP + multinucleated (≥3 nuclei) cells lining bone were scored as osteoclasts. The region of interest for histomorphometric analysis was limited to the furcal alveolar bone within the maxillary first molar trifurcation, excluding the periodontal ligament. The region of interest in the distal femur was limited to the secondary spongiosa, beginning 250 μm proximal to the growth plate and extending 1000 μm proximally, and 50 μm from endocortical surfaces. Images were taken at 400× for maxillary sections and 200× for femoral sections, acquired by Nikon's Inverted Microscope Eclipse TS100-F (Nikon Instruments, Inc., Melville, NY), and analyzed using NIH ImageJ software, version 1.51j8, https://imagej.nih.gov/ij/ (NIH, Bethesda, MD). Data are reported in accordance with standardized nomenclature[57], as previously described[13,44,55].

In situ immunofluorescence
In situ immunofluorescence analysis was carried out in paraffin-embedded sagittal sections of the maxillary first molar and sagittal sections of the distal femur. Specimens were deparaffinized with xylenes, rehydrated with graded ethanols, and washed with saline. Antigen retrieval was achieved in 10 mM sodium citrate buffer (pH 6.0). Samples were permeabilized in 1× PBS containing 0.2% Triton X-100 and blocked in 10% goat serum for one hour at room temperature. A 1:100 dilution of anti-osterix monoclonal antibody (clone sc #343396 Santa Cruz Biotechnology, Dallas, TX, USA) was incubated with specimens overnight at 4 °C. Sections were washed in 1X PBS and then incubated with a 1:2000 rhodamine-goat anti-mouse (Santa Cruz Biotechnology) for one hour at room temperature (protected from light). Samples were washed in 1× PBS and mounted via ProLong Diamond Antifade Mountant with DAPI (Life Technologies, Carlsbad, CA, USA). Images were acquired at 200X with a Keyence BZ-X810 fluorescence microscope. Images were stitched and overlaid with the Keyence BZ-X Analysis Software (Keyence, Osaka, Japan). Analysis of bone-lining osterix+ osteoblasts was determined in the maxillary first molar furcation alveolar bone. In the distal femur, analysis was limited to the secondary spongiosa, beginning 250 μm proximal to the growth plate, extending proximally 1000 μm, and 50 μm from endocortical surfaces. Images were scored using ImageJ software version 1.52a.

Bone marrow cultures
Femurs were isolated from each animal, and marrow was flushed using α-MEM media (Gibco, Fisher Scientific) + 20% Hyclone FBS + 1% 2 mM

glutamine + 100 U/ml penicillin + 100 mg/ml streptomycin (PSG). Bone marrow cells were disassociated, counted, and plated at 3×10^6 cells/cm^2 in a 60 mm dish as described previously[13,44,55]. Twelve hours later, the non-adherent hematopoietic progenitor cells (HPCs) were collected for osteoclast-precursor (OCP) assays. Fresh α-MEM media + 20% FBS + 1% PSG was added back to the cultures. Forty-eight hours later, adherent bone marrow mesenchymal stem cells (BMMSCs) were isolated for the osteoblast stimulation assay. Importantly, marrow cells were not combined from animals for initial bone marrow cultures or subsequent osteoclast-precursor/osteoblast assays; n-values reported for in vitro assays are representative of biological replicates.

In vitro osteoclast-precursor (OCP) assays
Non-adherent HPCs were collected from whole marrow cultures, washed, and labeled with CD11b microbeads (Miltenyi Biotec, Bergisch Gladbach, Germany). AutoMACS Sorter (Miltenyi Biotec) was used to separate CD11b$^-$ HPCs, as previously described[13,44,55]. CD11b$^-$ HPCs were plated at 1.5×10^5 cells/cm^2 in culture media (α-MEM media + 10% Hyclone FBS + 1% PSG) for assays; plated in 12-well plates for gene expression assays and 96-well plates for the TRAP stain assay. CD11b$^-$ HPCs were plated in culture media supplemented with 10 ng/mL CSF1 (R&D Systems; Minneapolis, MN), to enrich for CD11b$^-$ OCP cells having high osteoclast potential[13,44,55]. Thirty-six hours later, the culture media was changed. *Gene expression assay*: CD11b$^-$ OCP cells were stimulated with fresh control (25 ng/mL CSF1; R&D Systems) or treatment (25 ng/mL CSF1 + 50 ng/mL RANKL; R&D Systems) media for 4-days; media refreshed every other day. Day-4 CD11b$^-$ OCP cells were isolated for qRT-PCR gene expression analysis; performed in duplicate (technical replicate) cultures[13,44,55]. Data are representative of two separate experiments. *TRAP stain assay*: CD11b$^-$ OCP cells were stimulated with fresh control (25 ng/mL CSF1; R&D Systems) or treatment (25 ng/mL CSF1 + 50 ng/mL RANKL; R&D Systems) media for 6-days; media refreshed every other day. Day-6 cultures were stained by the TRAP method, as described previously[13,44,55]. Cytomorphometric analysis of TRAP$^+$ osteoclast cells was carried out in triplicate (technical replicate) cultures; five fields of view were analyzed per technical replicate culture at 100×. TRAP + cells with ≥3 nuclei were scored as an osteoclast[13,44,55]. Analysis was performed using NIH ImageJ software, version 1.51j8, https://imagej.nih.gov/ij/ (NIH, Bethesda, MD). Data are representative of two separate experiments.

In vitro osteoblast stimulation assay
BMMSCs were plated in culture media (α-MEM media + 10% Hyclone FBS + 1% PSG) at 2.0×10^4 cells/cm^2 in 12-well plates. Upon reaching confluency, cultures were stimulated with osteogenic media (α-MEM media + 10% Hyclone FBS + 1% PSG + 50 μg/ml ascorbic acid) for 5 days, media changed every other day. Cells were then cultured in serum-deprived osteogenic media (α-MEM media + 0.3% Hyclone FBS + 1% PSG + 50 μg/ml ascorbic acid) overnight. On Day-6, cultures were stimulated for 2 h with serum-deprived osteogenic media supplemented with either vehicle-control, IL17A (200 ng/mL, R&D Systems), or TNF (2 ng/mL, R&D Systems), as described previously[50,51]. After the 2-h stimulation, supernatants were aspirated, and cells were washed to remove recombinant cytokines. Fresh serum-deprived osteogenic media was added back to cultures for 6 h. Cell culture supernatants were then collected for ELISA protein assays and the in vitro osteoblast-osteoclast coupling assay, and cells were isolated for qRT-PCR gene expression analysis. In vitro osteoblast stimulation assay was performed in triplicate (technical replicate) cultures. Data are representative of two separate experiments.

In vitro osteoblast-osteoclast coupling assay
RAW264.7 murine macrophage cells were expanded in culture media (α-MEM media + 10% Hyclone FBS + 1% PSG). RAW264.7 cells were passed and plated at 1.5×10^5 cells/cm^2 in 96-well plates for the osteoblast-osteoclast coupling assay. RAW264.7 cells were plated in 100 μL culture media for 4-h and then supplemented with 100 μL of culture media containing 100 ng/ml RANKL (R&D Systems); final concentration of RANKL at 50 ng/ml. The cultures were not disturbed for 3 days, which allowed for the RAW264.7 cells to initiate fusing into small multinucleated cells.

On day-3, the culture media was changed in order to treat the RAW264.7 cells with supernatants derived from the in vitro osteoblast stimulation assay. The old media was aspirated and 100 μL of fresh culture media was added back to the cultures. 50 μL of osteoblast culture supernatant was immediately added to each culture, followed by 50 μL of fresh culture media containing 50 ng/ml RANKL; final concentration of RANKL at 25 ng/ml. Neutralizing antibodies αCXCL1 (500 pg/mL; R&D Systems) and αCCL2

(2000 pg/mL; R&D Systems) were added into cultures with supernatants derived from the in vitro osteoblast stimulation assay on day-3. Concentrations of αCXCL1 and αCCL2 neutralizing antibodies were based on outcomes from osteoblast supernatant ELISA assays.

Forty-eight hours later on day-5 of the culture system, the RAW264.7 cells were fixed and stained by the TRAP method. TRAP stain assay was carried out in triplicate (technical replicate) cultures. Images were acquired and technical replicate cultures were analyzed at 200X. TRAP$^+$ cell with ≥3 nuclei was scored an osteoclast for cytomorphometric analysis. Analysis was performed using NIH ImageJ software, version 1.51j8, https://imagej.nih.gov/ij/ (NIH, Bethesda, MD).

Prior to executing the investigations with osteoblast culture supernatants from experimental GF and SFB mice, optimization studies were performed with RAW264.7 cells and osteoblast culture supernatants derived from 11 to 12 week-old male specific-pathogen-free mice. Optimization studies discerned that culturing the RAW264.7 cells in 25 ng/ml RANKL from day-3 to day-5 of the culture system supported the formation of small TRAP$^+$ osteoclastic cells. Supplementing the cultures with 50 μL of osteoblast culture supernatant promoted the formation of larger TRAP$^+$ osteoclastic cells throughout the culture well.

qRT-PCR for 16S rDNA
Distal ileum contents and maxillary gingiva were harvested at euthanasia. Previous studies characterizing SFB colonization along the murine gastrointestinal tract have shown that SFB predominates in the distal/terminal ileum[58,59]. Therefore, the most distal 20 mm of the ileum was isolated for qRT-PCR assays assessing bacterial 16S rDNA and murine mRNA. Ileal contents were utilized for bacterial 16S rDNA analysis, and ileal tissue was used for murine mRNA analyses. Bacterial DNA was isolated from distal ileum contents and maxillary gingiva using the Qiagen DNeasy Powersoil Pro Kit, per manufacturer's protocols (Qiagen, Hilden, Germany). qRT-PCR protocol was executed on the StepOnePlus System (Applied Biosystems) for 30 cycles[55,60]. Universal 16S rDNA target gene was tested using the forward (Fwd) primer: 5′-ACT CCT ACG GGA GGC AGC AGT-3′, and reverse (Rev) primer: 5′-ATT ACC GCG GCT GGC-3′[44,55,60]. SFB was assessed via primers: Fwd: 5′-GAC GCT GAG GCA TGA GAG CAT-3′, Rev: 5′-GAC GGC ACG GAT TGT TAT TCA-3′, as described previously[44]. SFB rDNA from ileum and gingiva specimens of GF and SFB mice were normalized to a bacterial DNA standard (ZymoBIOMICS, Irvine, CA) as previously described[44]. Relative quantification of data was carried out by the $2^{-\Delta\Delta C_T}$ method[61,62]. All reactions were performed in duplicate.

Quantitative real-time PCR (qRT-PCR) for mRNA
Mandible bone marrow was flushed with TRIzol Reagent (Invitrogen, Carlsbad, CA). Mandibular mucogingival tissues were collected at euthanasia and homogenized in TRIzol. Distal ileum tissue was flash frozen, pulverized, and homogenized in TRIzol. Cell cultures were washed twice with 1X PBS, and TRIzol was directly applied to lyse cells. RNA was isolated by the TRIzol method following manufacturer's instructions, as previously described[13,44,55]. Total RNA was quantified via NanoDrop 1000 (Thermo Scientific, Waltham, MA). cDNA was produced using Taqman Random Hexamers and Reverse Transcription Reagents (Applied Biosystems, Foster City, CA), according to the manufacturer's protocol. cDNA was amplified using TaqMan gene expression primers/probes, Universal PCR Master Mix, and the StepOnePlus System (Applied Biosystems). Primers used included *Tnfrsf11a (Rank)*, *Dcstamp*, *Tnfsf11 (Rankl)*, *Tnfrsf11b (Opg)*, *Il17a*, *Tnf*, *Ccl2*, *Cxcl1*, *Cxcl5*, *Gapdh*, and *Rn18s*; all primers were purchased from Thermo Scientific. *Gapdh* was used as an endogenous control for ileum, mandible marrow, and cell culture specimens, and *Rn18s* was utilized as the endogenous control for mucogingival samples. Relative quantification of data was performed via the comparative C_T method ($2^{-\Delta\Delta C_T}$)[62,63], as previously described[13,44,55]. All reactions were performed in duplicate.

Flow cytometric analysis
Mandible bone marrow cells were isolated, washed, and counted as previously described[13,44,55]. *Live Cell Analysis*: Cells were treated with FcR-block (Miltenyi Biotec) and stained for cell surface markers. *CD4$^+$ Naïve/Activated T-cells*: Naïve/activated helper T-cells were gated on CD3$^+$ cells, followed by gating for helper T-cells (CD4$^+$CD8$^-$) or cytotoxic T-cells (CD4$^-$CD8$^+$). CD3$^+$CD4$^+$CD8$^-$ (Q1) were subsequently gated on naïve (CD62L$^+$CD69$^-$) or activated (CD62L$^-$CD69$^+$) surface markers; anti-CD3-PE-Vio770 (Miltenyi Biotec; clone REA641), anti-CD4-VioBlue (Miltenyi Biotec; clone REA604), anti-CD8-PE (Miltenyi Biotec; clone REA601), anti-CD62L-FITC (Miltenyi Biotec; clone REA828), anti-CD69-APC (Miltenyi Biotec; cloneH1.2F3).
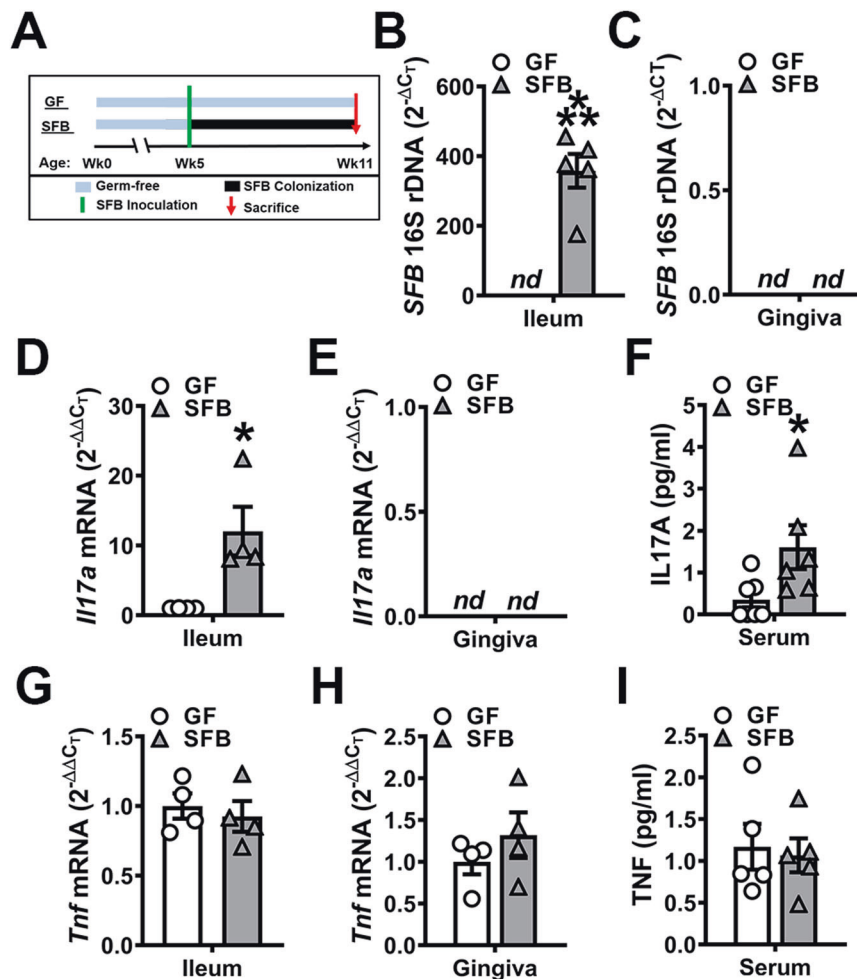
Fig. 1 SFB does not colonize or induce immune responses in oral mucogingival tissues. A Experimental timeline. Eleven-week-old male GF and SFB mice were euthanized, and specimens harvested for analysis. 16S rDNA analysis for SFB colonization; relative quantification of rDNA was performed via the CT method ($2^{-\Delta CT}$). **B** 16S rDNA analysis of SFB expression in distal ileum ($n = 5$/gp). **C** 16S rDNA analysis for SFB colonization in gingiva ($n = 5$/gp). *Il17a* mRNA qRT-PCR analysis; relative quantification of mRNA was performed via the $2^{-\Delta\Delta CT}$ method. **D** *Il17a* mRNA expression in ileums of GF vs. SFB mice ($n = 4$/gp). **E** *Il17a* mRNA expression in gingiva of GF vs. SFB mice ($n = 4$/gp). **F** Serum ELISA analysis of IL17A levels ($n = 6$/gp). *Tnf* mRNA qRT-PCR analysis; relative quantification of mRNA was performed via the $2^{-\Delta\Delta CT}$ method. **G** *Tnf* mRNA expression in ileums of GF vs. SFB mice ($n = 4$/gp). **H** *Tnf* mRNA expression in gingiva of GF vs. SFB mice ($n = 4$/gp). **I**. Serum ELISA analysis of TNF levels ($n = 5$/gp). Unpaired t test; data are presented as mean $\pm$ SEM, *$p < 0.05$, **$p < 0.01$, ***$p < 0.001$.

Dendritic cells (DCs): Dendritic cells were negatively gated on B220- cells, followed by examining cell surface markers MHC II$^+$CD11c$^+$ (Q2); anti-CD11c-PE-Vio770 (Miltenyi Biotec; clone REA754), anti-MHC II-FITC (Miltenyi Biotec; clone REA528), anti-B220-VioBlue (Miltenyi Biotec; clone REA755). Dead cells were excluded from analysis via propidium iodide viability dye (Miltenyi Biotec). *CD4$^\pm$ Helper T-cell Subset Analysis*: Cells were treated with FcR-block (Miltenyi Biotec) and stained for cell surface markers. Cells were then treated with fixation/permeabilization buffer (eBioscience) to label intracellular transcription factors. T$_{REG}$ *cells:* T$_{REG}$ cells were gated on CD3$^+$CD4$^+$ (Q2), followed by positive gating for CD25 and transcription factor FoxP3; anti-CD3-APC-Vio770 (Miltenyi Biotec; clone REA641), anti-CD4-FITC (Miltenyi Biotec; clone REA604), anti-CD25-PE-Vio770 (Miltenyi Biotec; clone 7D4), and anti-FoxP3-PE (Miltenyi Biotec; clone REA788). T$_H$1 *cells:* T$_H$1 cells were gated on CD3$^+$CD4$^+$ (Q2), followed by positive gating for CD183 and transcription factor T-bet; anti-CD3-PE-Vio770 (Miltenyi Biotec; clone REA641), anti-CD4-FITC (Miltenyi Biotec; clone REA604), anti-CD183-PE (Miltenyi Biotec; clone CXCR3-173), anti-T-bet-APC (Miltenyi Biotec; clone REA102). T$_H$2 *cells*: T$_H$2 cells were gated on CD3$^+$ cells, followed by positive gating of T$_H$2 surface markers CD4$^+$CD184$^+$. CD3$^+$CD4$^+$CD184$^+$ (Q2) were gated on transcription factors GATA3$^+$IRF4$^-$;anti-CD3-APC-Vio770 (Miltenyi Biotec; clone REA641), anti-CD4-FITC (Miltenyi Biotec; clone REA604), anti-CD184-PE-Vio770 (Miltenyi Biotec; clone REA107), anti-GATA3-PE (Miltenyi Biotec; clone REA174), anti-IRF4-APC (Miltenyi Biotec; clone REA201). T$_H$17 *cells:* T$_H$17 cells were gated on CD3$^+$ cells, followed by positive gating of T$_H$17 surface markers CD4$^+$CD196$^+$.

CD3$^+$CD4$^+$CD196$^+$ (Q2) were gated on transcription factors RORγt$^+$AHR$^-$; anti-CD3-APC-Vio770 (Miltenyi Biotec; clone REA641), anti-CD4-FITC (Miltenyi Biotec; clone REA604), anti-RORγT-APC (Miltenyi Biotec; clone REA278), anti-AHR-PE-Vio770 (eBioscience; clone 4MEJJ). Dead cells were excluded from analysis via e450 viability dye (Invitrogen). A minimum of 5000 gated cells were analyzed per specimen. Data were acquired by MACSQuant System (Miltenyi Biotec) and analyzed by FlowJo 11.0 software (TreeStar, Ashland, OR).

Enzyme-linked immunosorbent assays (ELISA)
Whole blood was collected via cardiac puncture at euthanasia, serum was isolated, and stored at $-80°C$. IL17A (Quantikine, R&D Systems), TNF (Quantikine, R&D Systems), P1NP (Immunodiagnostics Systems Inc, Gaithersburg, MD, USA), and TRAP5b (Immunodiagnostics Systems Inc) were assessed in serum isolates. CXCL1 (Quantikine, R&D Systems), CCL2 (Quantikine, R&D Systems), and CXCL5 (Quantikine, R&D Systems) was evaluated in osteoblast culture supernatants. ELISA kits were used following manufacturer's protocols. All reactions were performed in triplicate.

Statistical analysis
Power analysis was performed in consultation with the Biostatistical Unit of the Medical University of South Carolina Bioinformatics Core and was established on the authors' previous studies utilizing gnotobiotic murine models. Unpaired t tests or 2-way ANOVA with Tukey Post Hoc tests were
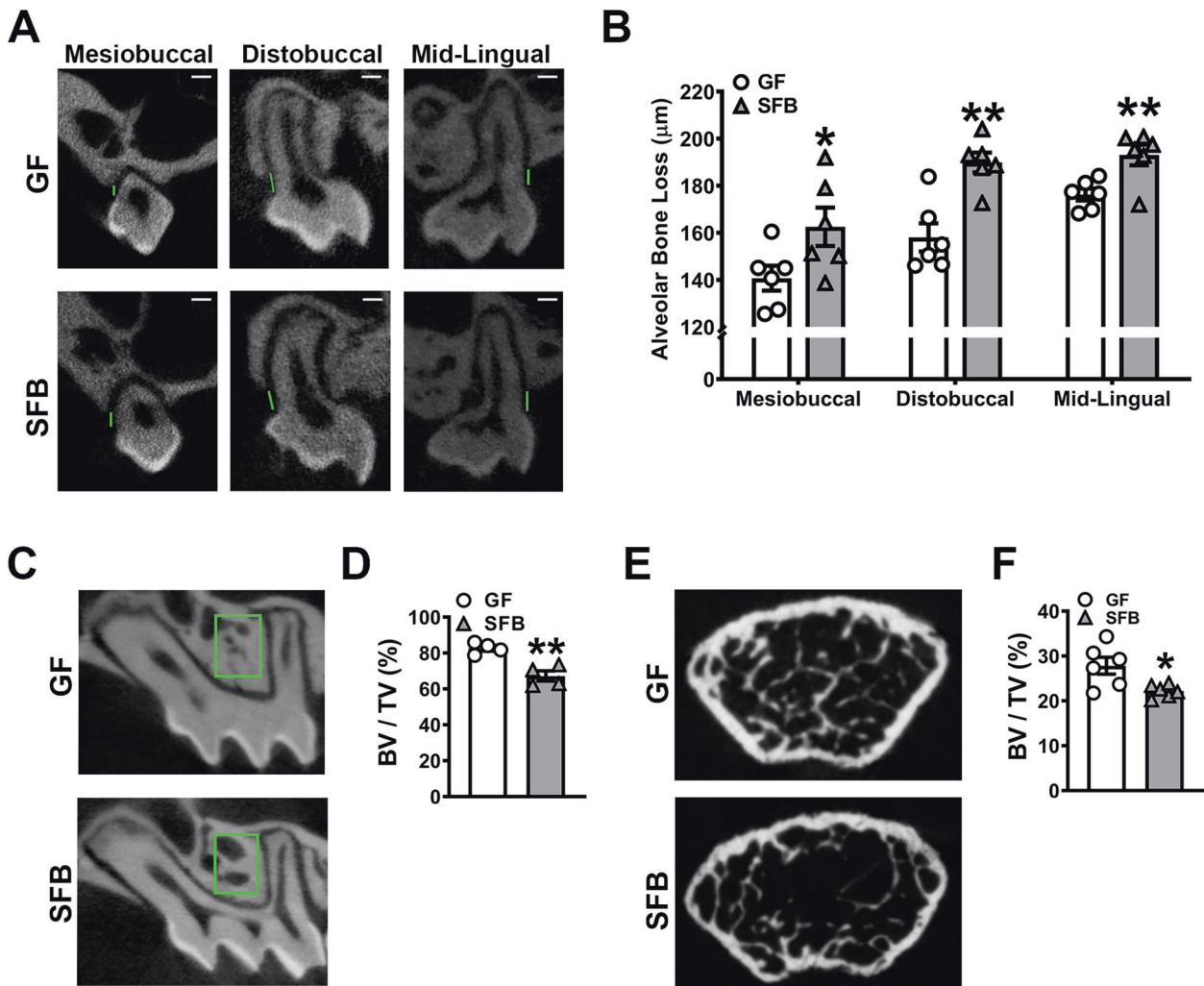
Fig. 2 SFB has catabolic effects on alveolar bone. Alveolar bone loss was measured by calculating the linear distance between the cementoenamel junction (CEJ) and alveolar bone crest (ABC) at the maxillary first molar in reconstructed micro-CT images. **A** Representative micro-CT images displaying CEJ-ABC linear distance (green line) at the mesiobuccal line angle, distobuccal line angle, and mid-lingual aspect of the maxillary first molar; scale bar (white line) = 200 μm. **B** Quantitative measures of CEJ-ABC linear distance at the mesiobuccal line angle, distobuccal line angle, and mid-lingual aspect of the maxillary first molar ($n = 6$/gp). **C** Representative micro-CT images of trabecular bone in the maxillary first molar trifurcation, region of interest outlined (green box). **D** Micro-CT quantitative analysis of trabecular bone volume per tissue volume (BV/TV) in the maxillary first molar furcal alveolar bone ($n = 4$/gp). **E** Representative micro-CT reconstructed cross-sectional images of trabecular bone in the distal femur, extending 50 μm proximally from where analysis began. **F** Micro-CT quantitative analysis of BV/TV in the distal femur ($n = 6$/gp). Unpaired t test; data are presented as mean ± SEM; $*p < 0.05$, $**p < 0.01$.

performed using GraphPad Prism 8.0 (La Jolla, CA, USA). Data are presented as mean ± SEM. Significance is designated as $p < 0.05$.

RESULTS
SFB does not colonize or induce immune responses in oral mucogingival tissues
SFB inoculation was strategically performed in 5-week-old weanling GF mice to generate SFB-monoassociated mice. GF and SFB mice were intentionally euthanized at age 11-weeks (Fig. 1A). The rationale for the experimental timeline was based on prior investigations in the SFB-monoassociated mouse model[29,32,64] and murine alveolar bone development[65–67]. When young GF mice are inoculated with SFB, host immune response effects are typically induced within 1–2 weeks and persist for at least 2 months[29,32,64]. Different from non-oral skeletal sites, alveolar bone formation is dependent on the development and eruption of the teeth[67,68]. Teeth are typically fully erupted and alveolar bone formation is complete in mice by age 5-weeks[65–67].

16S rDNA analysis demonstrated the presence of SFB in the ileum (Fig. 1B), but not in the oral cavity (Fig. 1C), of SFB-monoassociated mice. SFB induction of T_H17/IL17A-mediated immunity within the gut was validated by increased *Il17a* expression in the distal ileum of SFB vs. GF mice (Fig. 1D). *Il17a* expression was not detected in barrier mucogingival tissues (Fig. 1E), which corroborates prior findings that SFB does not colonize the oral cavity or induce T_H17/IL17A immunity in the gingiva[69]. Serum IL17A levels were enhanced in SFB vs. GF mice (Fig. 1F). SFB interactions with the host have been reported to upregulate TNF expression in intestinal cells[45–47]. Therefore, alterations in *Tnf*/TNF were analyzed in mucosal barrier tissues and the circulation (Fig. 1G-I). There were no differences in *Tnf* expression in the ileum (Fig. 1G) or mucogingival tissues (Fig. 1H). Furthermore, circulating TNF levels were similar in GF and SFB mice (Fig. 1I).

SFB has catabolic effects on alveolar bone
Micro-CT analysis was carried out to elucidate SFB-induced tissue level alterations in the skeleton (Fig. 2). Alveolar bone loss was examined at the maxillary first molar by measuring the linear
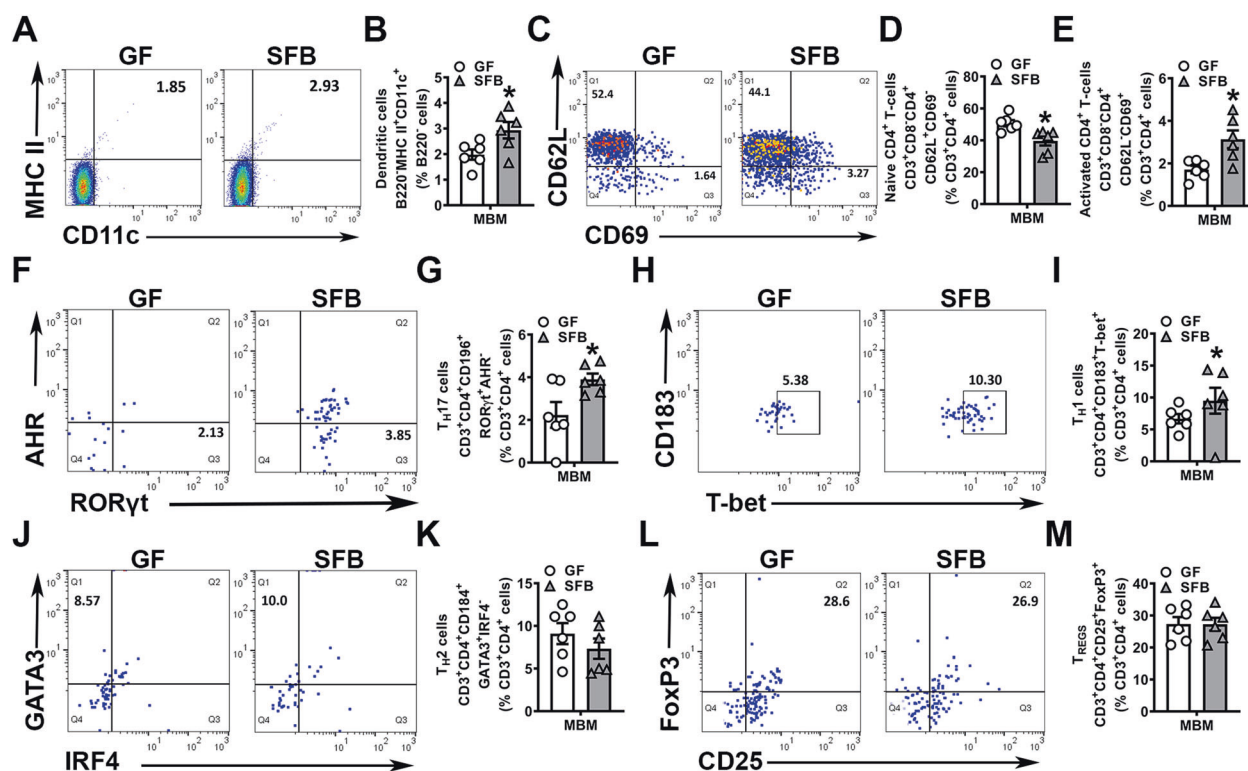
Fig. 3 **SFB upregulates immune response effects in alveolar bone marrow.** Mandible bone marrow (MBM) cells were isolated and stained for flow cytometric analysis ($n = 6$/gp); cell percentages are expressed relative to the appropriate gated population. **A** Representative gating of B220$^-$MHC II$^+$CD11c$^+$ dendritic cells (DCs). **B** Frequency of B220$^-$MHC II$^+$CD11c$^+$ DCs, gated on % B220$^-$ cells. **C** Representative gating of CD4 + naïve and activated T-cells. **D** Frequency of CD3$^+$CD8$^-$CD4$^+$CD62L$^+$CD69$^-$ naïve T-cells, gated on % CD3$^+$CD4$^+$ cells. **E** Frequency of CD3$^+$CD8$^-$CD4$^+$CD62L$^-$CD69$^+$ activated T-cells, gated on % CD3$^+$CD4$^+$ cells. **F** Representative gating of CD3$^+$CD4$^+$RORγt$^+$AHR$^-$ T$_H$17 cells. **G** Frequency of CD3$^+$CD4$^+$RORγt$^+$AHR$^-$ T$_H$17 cells, gated on % CD3$^+$CD4$^+$ cells. **H** Representative gating of CD3$^+$CD4$^+$CD183$^+$T-bet$^+$ T$_H$1 cells. **I** Frequency of CD3$^+$CD4$^+$CD183$^+$T-bet$^+$ T$_H$1 cells, gated on % CD3$^+$CD4$^+$ cells. **J** Representative gating of CD3$^+$CD4$^+$CD184$^+$GATA3$^+$ IRF4$^-$ T$_H$2 cells **K** Frequency of CD3$^+$CD4$^+$CD184$^+$GATA3$^+$ IRF4$^-$ T$_H$2 cells, gated on % CD3$^+$CD4$^+$ CD184$^+$ cells. **L** Representative gating of CD3$^+$CD4$^+$CD25$^+$FoxP3$^+$ T$_{REG}$ cells. **M** Frequency of CD3$^+$CD4$^+$CD25$^+$FoxP3$^+$ T$_{REG}$ cells, gated on % CD3$^+$CD4$^+$ cells. Unpaired t-test; data are presented as mean ± SEM, *$p < 0.05$, **$p < 0.01$.

distance from the cementoenamel junction (CEJ) to the alveolar bone crest (ABC) (Fig. 2A, B) and by analyzing the trabecular bone volume fraction in the trifurcation (Fig. 2C, D). The presence of SFB exacerbated linear alveolar bone loss at the mesiobuccal, distobuccal, and mid-lingual line angles (Fig. 2A, B; Supp Fig. 1) and blunted the trabecular bone volume fraction in the furcal alveolar bone (Fig. 2C, D).

Micro-CT morphometric analysis of the femur showed that SFB-induced bone loss is not specific to oral skeletal sites. Trabecular bone volume fraction was diminished by 18.6% in the maxillary first molar trifurcation (Fig. 2C, D) and by 20% in the distal femur (Fig. 2E, F) of SFB vs. GF mice. The reduced trabecular bone volume outcomes found in the distal femur of male SFB vs. GF mice reported herein (Fig. 2E, F) are similar to outcomes found in the proximal tibia of female SFB vs. GF mice[44].

SFB upregulates innate/adaptive immune response effects in alveolar bone

SFB induces T$_H$17/IL17A-mediated immunity in the lamina propria through the presentation of antigens by intestinal dendritic cells[33]. Furthermore, SFB has been shown to induce IL17A-dependent protection against intestinal pathogens via extraintestinal effects on bone marrow dendritic cells[39]. Recent osteoimmunology studies have discerned that SFB upregulates CD4$^+$ helper T-cell subsets in the bone marrow at non-oral skeletal sites[44,45]. However, it is unknown whether SFB influences helper T-cell-mediated immunity in the alveolar bone complex. Therefore, flow cytometric analysis of mandibular bone marrow cells was

performed to evaluate dendritic cells, activated and naïve CD4$^+$ T-cells, and CD4$^+$ helper T-cell subsets (Fig. 3).

The frequency of dendritic cells in the mandibular bone marrow was elevated in SFB vs. GF mice (Fig. 3A, B), which supports the notion that SFB-derived circulating mediators alter bone marrow dendritic cells[39]. In line with the expanded dendritic cell population found in SFB mice (Fig. 3A, B), naïve CD4$^+$ T-cells were decreased (Fig. 3C, D) and activated CD4$^+$ T-cells were increased (Fig. 3C, E) in the mandible bone marrow of SFB vs. GF mice. CD4$^+$ helper T-cell subset analysis revealed increased T$_H$17 cells (Fig. 3F, G) and T$_H$1 cells (Fig. 3H, I), but no differences in T$_H$2 cells (Fig. 3J, K) or T$_{REG}$ cells (Fig. 3L, M), in the mandible bone marrow of SFB vs. GF mice. Research has discerned that activated CD4$^+$ T-cells support bone-resorbing osteoclasts[15,70,71] and T$_H$17 cells have pro-osteoclastic actions that drive alveolar bone loss[72–74]. Considering that SFB colonization increased activated CD4$^+$ T-cells (Fig. 3C, E) and T$_H$17 cells (Fig. 3F, G) in mandible bone marrow, the reduced alveolar bone phenotype found in SFB mice (Fig. 2A–D) may be attributed to alterations in osteoclastogenesis.

SFB colonization does not alter osteoblastogenesis

Skeletal bone loss occurs when the actions of bone-resorbing osteoclasts exceed those of bone-forming osteoblasts[15,17]. Osteoblastic cell alterations were evaluated by in situ immunofluorescence analysis of osterix+ bone-lining osteoblast cells in the maxillary alveolar bone (Fig. 4A–C) and distal femur trabecular bone (Fig. 4D–F). SFB colonization did not affect osteoblast cell numbers or interface with alveolar bone in the maxillary first molar
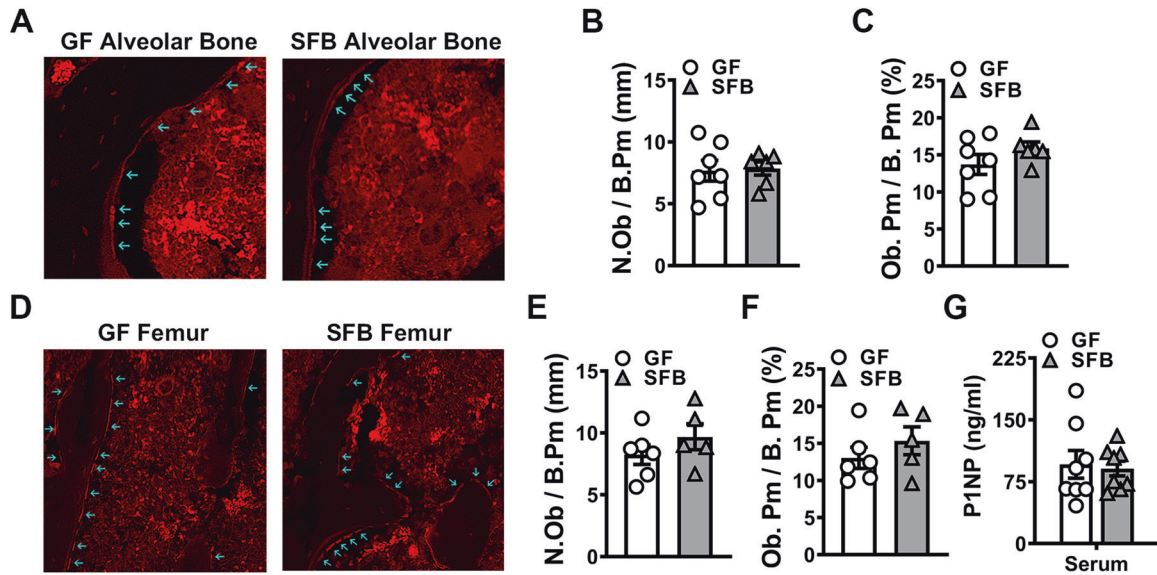
Fig. 4 SFB colonization does not alter osteoblastogenesis. Immunofluorescent analysis of osteoblasts in the maxillary first molar furcal alveolar bone ($n = 6$–7/gp). Osterix+ cuboidal cells lining bone were designated as osteoblasts (red, osterix – Rhodamine). **A** Representative image of osterix + osteoblasts lining the maxillary first molar furcal alveolar bone; arrows indicate labeled osteoblasts (200X). **B** N.Ob/B.Pm = osteoblast number per bone perimeter. **C** Ob.Pm/B.Pm = osteoblast perimeter per bone perimeter. Immunofluorescent analysis of osteoblasts in the secondary spongiosa of distal femur ($n = 5$–6/gp). Osterix+ cuboidal cells lining bone were designated as osteoblasts (red, osterix – Rhodamine). **D** Representative images of osterix+ osteoblasts lining the secondary spongiosa trabecular bone of distal femur; arrows indicate labeled osteoblasts (200×). **E** N.Ob/B.Pm. **F** Ob.Pm/B.Pm. **G** Serum ELISA analysis of P1NP levels ($n = 8$/gp). Unpaired t test; data are reported as mean ± SEM.

furcation (Fig. 4A–C) or the distal femur (Fig. 4D–F). Serum P1NP, a marker for osteoblast-mediated bone formation, was not different in SFB vs. GF mice (Fig. 4G), which suggests that SFB colonization does not alter osteoblast function across skeletal sites.

SFB colonization enhances osteoclastogenesis
To elucidate whether the presence of SFB impacted osteoclastogenesis in the alveolar bone complex, histomorphometric analysis of TRAP+ osteoclastic cells lining alveolar bone was performed in the furcation of the maxillary first molar (Fig. 5A–D). Whereas osteoclast numbers were similar (Fig. 5A, B), the osteoclast size was larger (Fig. 5A, C) in the alveolar bone of SFB vs. GF mice. The larger osteoclast size (Fig. 5A, C) contributed to an increased osteoclast perimeter per bone perimeter (Fig. 5A, D) at the alveolar bone surface of SFB mice. TRAP+ osteoclastic cell analysis in the femoral trabecular bone demonstrated that SFB actions promoting osteoclastogenesis are not specific to alveolar bone (Fig. 5E–H). SFB mice had increased osteoclast numbers (Fig. 5E, F) and a trend toward larger osteoclast size (Fig. 5E, G), which contributed to an enhanced osteoclast perimeter per bone perimeter (Fig. 5E, H), in the distal femur. Serum TRAP5B levels were higher in SFB vs. GF mice (Fig. 5I), which supports that SFB colonization increases osteoclastogenesis across skeletal sites.

OCP cell in vitro differentiation assays were employed to further investigate SFB effects on osteoclastogenesis (Fig. 5J–N). Magnetic cell sorting was used to enrich for marrow CD11b⁻ HPCs, which are monocyte progenitor cells. CD11b⁻ HPCs were primed in culture with CSF1 to drive the cells down the OCP lineage[75,76]. CD11b⁻ OCP cultures were stimulated with control media (25 ng/ mL CSF1) or treatment media (25 ng/mL CSF1 + 50 ng/mL RANKL) for 4 or 6 days. Day-6 in the CD11b⁻ OCP culture system is when terminal osteoclast maturation occurs[44,55]. Therefore, day-6 OCP cultures were TRAP stained for osteoclast cytomorphometric analysis (Fig. 5J–M). CD11b⁻ OCPs were isolated from day-4 OCP cultures for qRT-PCR analysis to target osteoclastic genes (Fig. 5N) implicated in cell level alterations found in day-6 OCP cultures. While osteoclast numbers were not different (Fig. 5J, K), osteoclast

size (Fig. 5J, L) and number of nuclei per osteoclast (Fig. 5J, M) were increased in day-6 CD11b⁻ OCP cultures from SFB vs. GF mice. Treatment over control analysis was carried out in RANKL + CSF1 treatment cultures relative to CSF1 control cultures to assess alterations in *Dcstamp*, a RANKL-induced transmembrane protein critical for osteoclast fusion[77,78]. RANKL treatment promoted a greater induction of *Dcstamp* in SFB vs. GF CD11b⁻ OCP cultures (Fig. 5N), which delineates that SFB immunomodulation supports RANKL-induced osteoclast fusion.

In vivo gene expression studies were performed in mandible bone marrow to delineate immunoregulatory mechanisms mediating SFB actions supporting osteoclastogenesis. *Rank* and the *Rankl:Opg* ratio were evaluated to assess alterations in the RANKL signaling axis (Fig. 5O, P). When investigating alterations in RANKL signaling at the RANK receptor, the RANKL/OPG ratio must be evaluated to account for changes in the endogenous decoy receptor, osteoprotegerin (OPG)[75,76]. *Rank (Tnfrsf11a)* levels (Fig. 5O) and the *Rankl (Tnfsf11)/Opg (Tnfrsf11b)* ratio (Fig. 5P) were similar in the mandible bone marrow of GF and SFB mice. These data suggest that SFB's pro-osteoclastic actions are not meditated by alterations in RANKL signaling at the RANK receptor. Appreciating that paracrine signaling effects in the bone marrow modulate RANKL-induced osteoclastogenesis, *Tnf* levels were assessed in the mandible bone marrow of GF and SFB mice. TNF is a proinflammatory cytokine that potently enhances RANKL-mediated osteoclastogenesis[70,71,79]. The rationale for assessing alterations in *Tnf* within the alveolar bone marrow was based on the knowledge that SFB colonization upregulates TNF in the bone marrow at non-oral skeletal sites[45]. *Tnf* was greater than threefold higher in the mandible bone marrow of SFB vs. GF mice (Fig. 5Q).

SFB induces osteoblast-derived signaling factors that support osteoclastogenesis
Osteoimmunology research has discerned that IL17A- and TNF-expressing T-cells in the bone marrow are increased due to inflammatory conditions in the gut[80] and the presence of SFB[45]. The current report has shown that SFB colonization in the gut
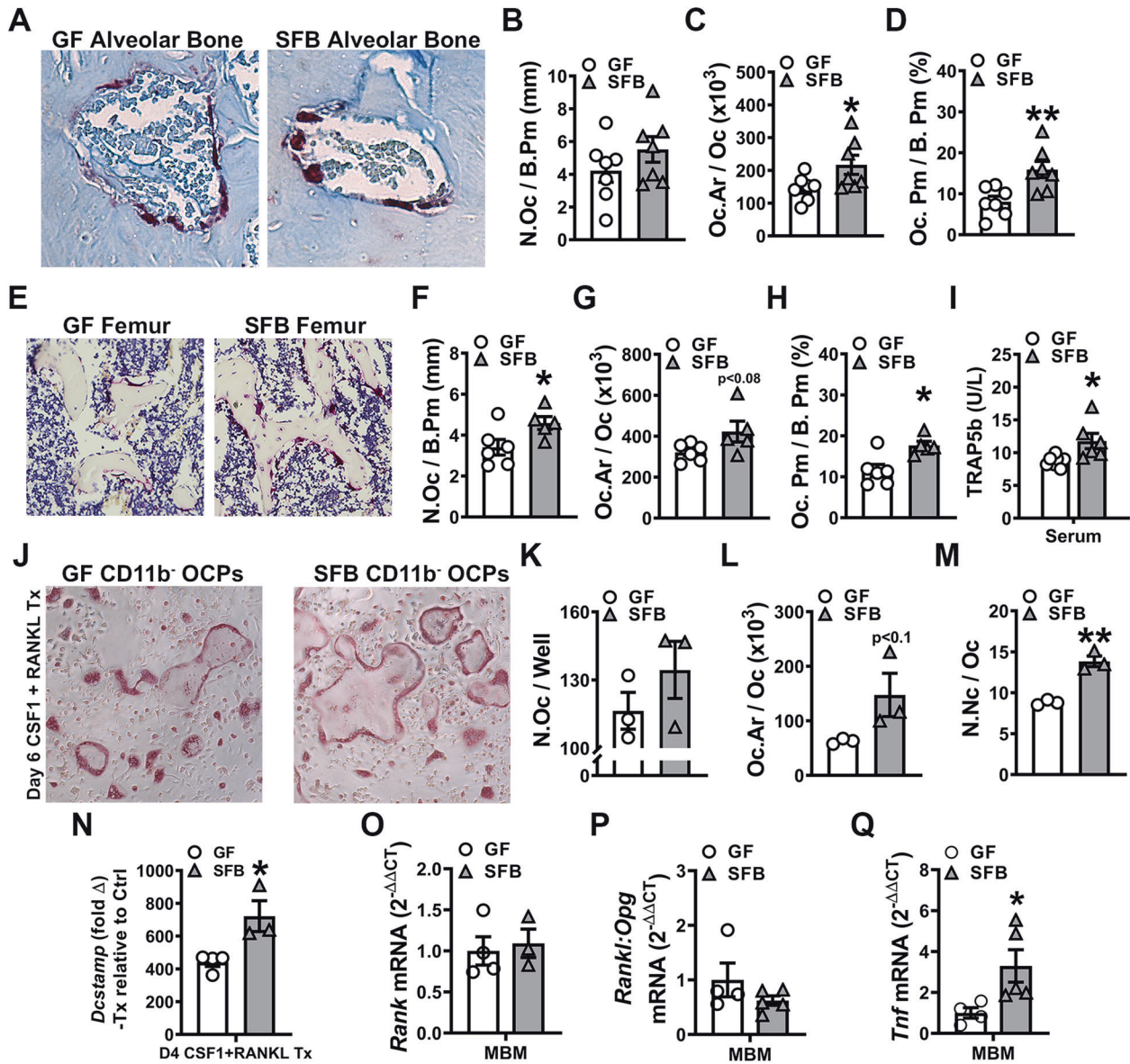
J.D. Hathaway-Schrader et al.

Fig. 5 SFB colonization enhances osteoclastogenesis. Maxillae harvested for histomorphometric analyses; sagittal sections cut and stained ($n = 7$/gp). Histomorphometric analyses of TRAP+ osteoclast cellular endpoints were performed in the maxillary first molar furcal alveolar bone. TRAP+ cells lining bone with ≥3 nuclei were designated an osteoclast. **A** Representative images of TRAP furcal alveolar bone (400X). **B** N. Oc/B.Pm = osteoclast number per bone perimeter. **C** Oc.Ar/Oc = average osteoclast area. **D** Oc.Pm/B.Pm = osteoclast perimeter per bone perimeter. Femurs were harvested for histomorphometric analyses; sagittal sections cut and stained ($n = 5$–6/gp). Histomorphometric analyses of TRAP + osteoclast cellular endpoints were performed in the secondary spongiosa of the distal femur. TRAP+ cells lining bone with ≥3 nuclei were designated an osteoclast. **E** Representative images of TRAP distal femur (200×). **F** N.Oc/B.Pm. **G** Oc.Ar/Oc. **H** Oc.Pm/B.Pm. **I** Serum ELISA analysis of TRAP5b levels ($n = 6$–7/gp). Day-6 OCP culture TRAP stain assay ($n = 3$/gp). **J** Representative images (100X) of CD11b- OCP cultures stimulated with treatment (CSF1 & RANKL) media for 6 days. **K** N.Oc/Well = number of osteoclasts per well. **L** Oc.Ar/Oc = average osteoclast area. **M** N.Nc/Oc = nuclei number per osteoclast. **N** qRT-PCR gene expression studies were carried out in Day-4 CD11b- OCP cultures to detect early transcription level alterations in RANKL-stimulated osteoclast differentiation ($n = 3$–4/gp). Relative quantification of *Dcstamp* mRNA was performed by the $2^{-\Delta\Delta C_T}$ method; data expressed as treatment (CSF1 and RANKL) fold change relative to control (CSF1). Mandible bone marrow (MBM) qRT-PCR analysis of (**O**) *Tnfrsf11a (Rank)* mRNA, **P** *Tnfsf11(Rankl):Tnfrsf11b(Opg)* ratio and (**Q**) *Tnf* mRNA ($n = 3$–5/gp). Relative quantification of mRNA was performed via the $2^{-\Delta\Delta C_T}$ method. Unpaired *t* test; data are presented as mean ± SEM, *$p < 0.05$, **$p < 0.01$.

upregulates circulating IL17A levels (Fig. 1E) and increases the frequency of T$_H$17 cells in alveolar bone marrow (Fig. 3F, G). Furthermore, activated CD4+ T-cells (Fig. 3C, E) and *Tnf* (Fig. 5Q) were enhanced in the alveolar bone marrow of SFB vs. GF mice. IL17A and TNF signaling at osteoblastic cells promotes the synthesis of pro-osteoclastic chemokines/cytokines that support bone osteolysis[48–53]. Therefore, we established an in vitro osteoblast-osteoclast coupling assay targeting IL17A and TNF signaling effects on primary osteoblastic cells to elucidate whether

SFB pro-osteoclastic actions are mediated through osteoblast-osteoclast crosstalk.

First passage confluent BMMSCs from GF and SFB mice were cultured in osteogenic media to drive the cells down the osteoblastic lineage. Osteoblast cultures were then subjected to a single treatment with vehicle-control (VEH-Ctrl), IL17A, or TNF. Two hours later, the supernatants were aspirated, and cultures were washed to remove the recombinant cytokines. Fresh media was added back to the osteoblast cultures to allow for the
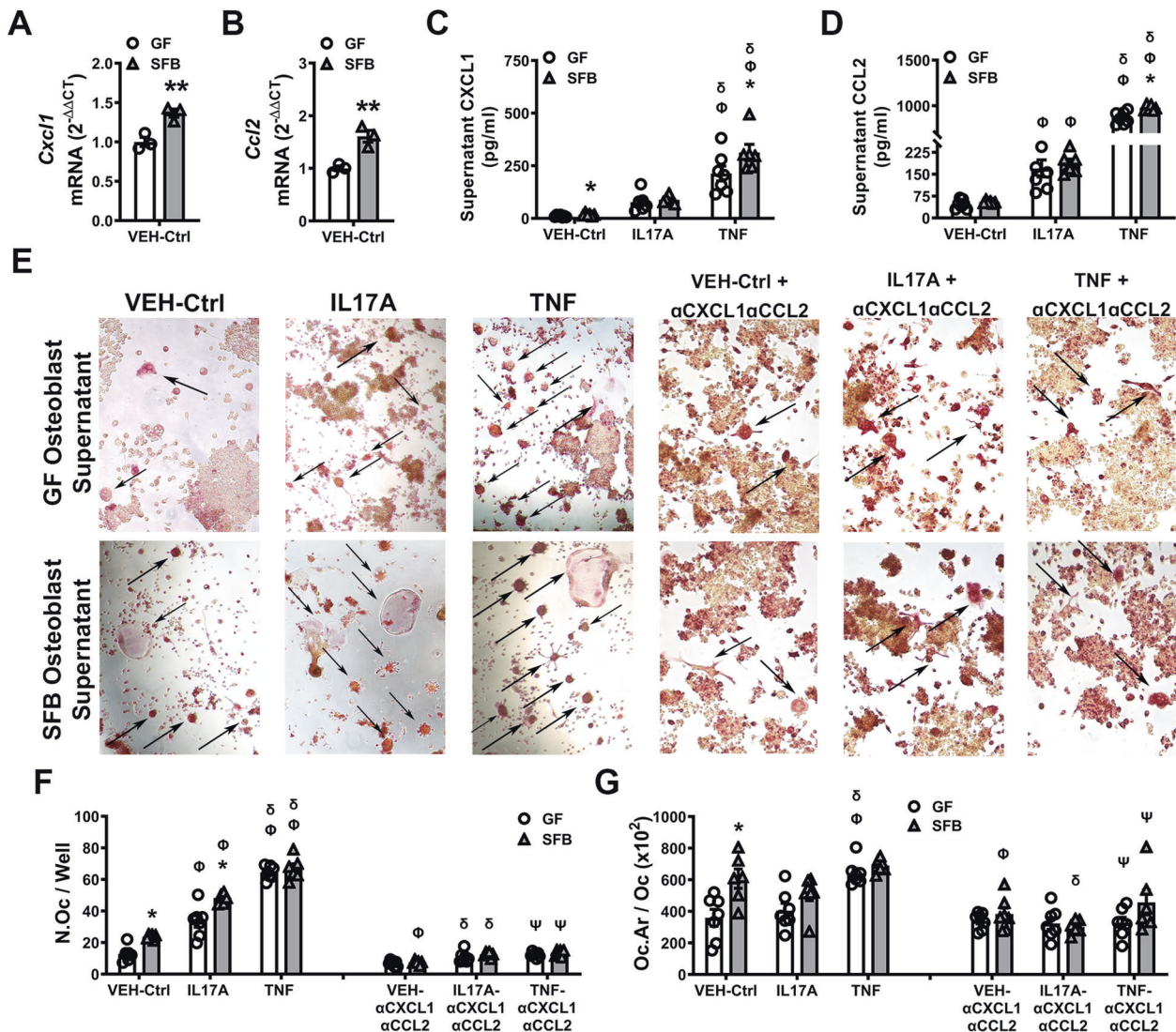
Fig. 6 SFB induces osteoblast-derived signaling factors that support osteoclastogenesis. Osteoblast (OB) cultures were stimulated with vehicle-control (VEH-Ctrl), IL-17A, or TNF. OB cells were isolated for qRT-PCR gene expression analysis. OB supernatants were collected for ELISA protein analysis and the in vitro osteoblast-osteoclast coupling assay. RNA was isolated from VEH-Ctrl-stimulated OBs for qRT-PCR analysis of (**A**) *Cxcl1* and (**B**) *Ccl2* mRNA ($n = 3$/gp); relative quantification of mRNA was performed via the $2^{-\Delta\Delta CT}$ method. Unpaired t test; data are presented as mean $\pm$ SEM, **$p < 0.01$. OB supernatant ELISA analysis of (**C**) CXCL1 and (**D**) CCL2 levels ($n = 6$–7/gp). Osteoblast-osteoclast coupling assay. RANKL-induced RAW264.7 osteoclast cells were stimulated with supernatants from VEH-Ctrl-, IL17A-, or TNF-treated OBs $\pm$ αCXCL1 and αCCL2 neutralizing antibodies on day-3. TRAP stain was performed on day-5 of the culture system; TRAP$^+$ cells with $\geq$3 nuclei were designated an osteoclast ($n = 6$–7/gp). **E** Representative images (200X) of TRAP$^+$ RAW264.7 osteoclast cells stimulated with supernatants from VEH-Ctrl-, IL17A-, or TNF-treated OBs $\pm$ αCXCL1 and αCCL2 neutralizing antibodies. **F** N.Oc/Well = number of osteoclasts per well. **G** Oc. Ar/Oc = average osteoclast area. Two-way ANOVA with Tukey post hoc test; data are presented as mean $\pm$ SEM. *$p < 0.05$ between treatment-matched GF vs. SFB groups; $^\Phi p < 0.05$ vs. VEH-Ctrl (group-matched); $^\delta p < 0.05$ vs. IL17A treatment (group-matched); $^\Psi p < 0.05$ vs. TNF treatment (group-matched).

secretion of pro-osteoclastic factors. Six hours later, the culture supernatants were collected for the in vitro osteoblast-osteoclast coupling assay and ELISA protein analysis. Osteoblast cells were isolated for qRT-PCR gene expression analysis.

To begin elucidating the molecular underpinnings of SFB actions on osteoblast-osteoclast crosstalk, qRT-PCR gene expression studies were performed in osteoblast cell lysates (Fig. 6A, B; Supp Fig. 2A–E). The pro-osteoclastic factors, CXCL1, CCL2, and CXCL5 were purposely targeted, since they are IL17A and TNF responsive genes in osteoblasts[50,51,81,82]. *Cxcl1* (Fig. 6A) and *Ccl2* (Fig. 6B) mRNA were increased, whereas there were no differences in *Cxcl5* expression (Supp Fig. 2A), in VEH-Ctrl-treated osteoblasts from SFB vs. GF mice. IL17A- and TNF-induced fold change increases in *Cxcl1* (Supp Fig. 2B), *Ccl2* (Supp Fig. 2C), and *Cxcl5*

(Supp Fig. 2D) were consistent in osteoblasts derived from SFB vs. GF mice. qRT-PCR studies were also performed in SFB vs. GF osteoblast culture lysates, which ruled out differences in the *Rankl: Opg* axis (Supp Fig. 2E).

Appreciating that protein levels of osteoblast-derived cytokines critically regulate osteoblast-osteoclast crosstalk, supernatants from osteoblast cultures treated with VEH-Ctrl, IL17A, and TNF were assessed for differences in CXCL1 (Fig. 6C, Supp Table 1), CCL2 (Fig. 6D, Supp Table 2), and CXCL5 (Supp Fig. 2F). CXCL1 (Fig. 6C) was increased in VEH-Ctrl-treated osteoblast culture supernatants from SFB vs. GF mice, while there no differences in unstimulated levels of CCL2 (Fig. 6D) and CXCL5 (Supp Fig. 2F). Compared to VEH-Ctrl treatment, IL17A treatment-induced SFB and GF osteoblasts to secrete higher levels of CCL2 (Fig. 6D).
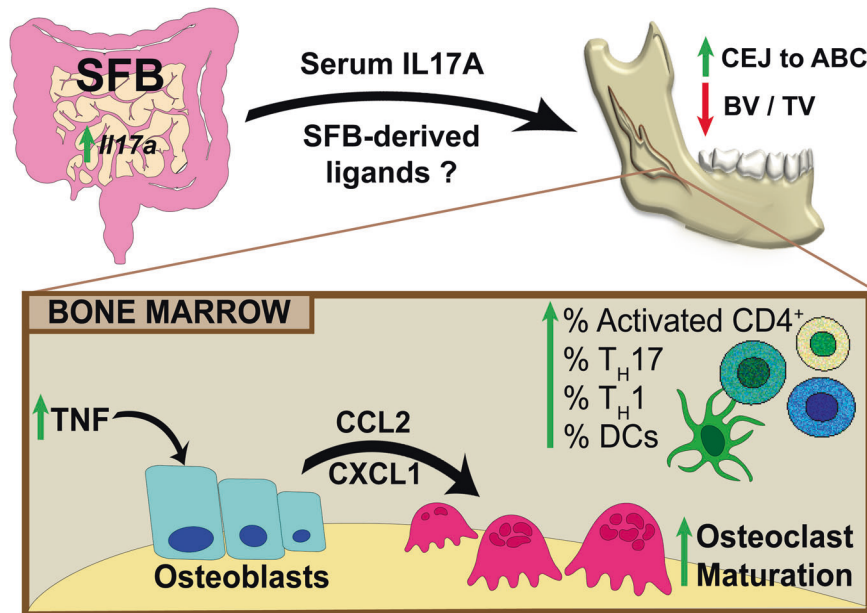
Fig. 7 **Schematic of SFB immunomodulatory actions on skeletal health.** SFB colonization of the gut has immunomodulatory actions, which impairs trabecular bone microarchitecture at oral and non-oral skeletal sites. SFB elevates IL17A in the ileum and serum and potentially increases bacterial antigens/ligands in circulation, which have immunoregulatory effects on alveolar bone. Importantly, SFB increased TNF expression in the alveolar bone marrow microenvironment. TNF signaling at osteoblastic cells induced CXCL1 and CCL2 secretion which enhanced osteoclastogenesis. Therefore, commensal gut microbes have the capacity to regulate osteoimmune responses and skeletal homeostasis in alveolar bone.

However, the upregulated CCL2 levels were similar in IL17A-treated osteoblast cultures from SFB vs. GF mice (Fig. 6D). Relative to VEH-Ctrl or IL17A treatment, TNF treatment-induced SFB and GF osteoblasts to secrete substantially higher levels of CXCL1 (Fig. 6C) and CCL2 (Fig. 6D). The increased levels of CXCL1 (Fig. 6C) and CCL2 (Fig. 6D) were greater in TNF-treated osteoblast cultures from SFB vs. GF mice. IL17A treatment and TNF treatment did not modulate CXCL5 levels in SFB or GF osteoblast cultures (Supp Fig. 2F).

The osteoblast-osteoclast coupling assay was performed by stimulating RANKL-induced RAW264.7 osteoclastic cells with osteoblast culture supernatants from GF and SFB mice (Fig. 6E–G; Supp Tables 3,4). Based on our findings that secreted levels of CXCL1 (Fig. 6C) and CCL2 (Fig. 6D) were different in SFB vs. GF osteoblast culture supernatants, blocking antibodies were employed to elucidate the role of these factors in SFB immunomodulation of osteoblast-osteoclast crosstalk. Supernatants from VEH-Ctrl-treated SFB osteoblasts compared to VEH-Ctrl-treated GF osteoblasts induced the formation of larger numbers of RAW264.7 osteoclast cells (Fig. 6F), which were greater in size (Fig. 6G). The addition of αCXCL1 + αCCL2 neutralizing antibodies reduced the osteoclast numbers and size in cultures stimulated with VEH-Ctrl-treated SFB osteoblast supernatants, which normalized osteoclast outcomes driven by VEH-Ctrl-treated osteoblast supernatants (Fig. 6F, G). These outcomes imply that CXCL1 and CCL2 support SFB actions promoting basal levels of osteoclastogenesis. Relative to supernatants from VEH-Ctrl-treated osteoblasts, supernatants from IL17A-treated osteoblasts increased osteoclast cell numbers, and this increase was greater in osteoblasts from SFB vs. GF mice (Fig. 6F, G). The αCXCL1 + αCCL2 neutralizing antibodies attenuated the enhanced osteoclast cell numbers driven by the IL17A-treated osteoblast supernatants (Fig. 6F, G). Supernatants from TNF-treated GF osteoblasts vs. VEH-Ctrl-treated and IL17A-treated GF osteoblasts induced greater numbers of osteoclastic cells (Fig. 6F), which were larger in size (Fig. 6G). Notably, osteoclast outcomes were similar in RAW264.7 osteoclast cells stimulated with supernatants from TNF-treated GF osteoblasts and TNF-treated SFB osteoblasts (Fig. 6B–D). The presence of αCXCL1 + αCCL2 neutralizing antibodies

blocked the increased osteoclast cell numbers and size driven by the TNF-treated GF osteoblast supernatants. These findings support the notion that TNF signaling at osteoblastic cells promotes SFB-induced pro-osteoclastic actions through the induction of CXCL1 and CCL2.

DISCUSSION
Four decades ago, researchers monoassociated GF rats with different commensal oral bacteria to show that commensal oral microbes critically regulate alveolar bone homeostasis[18–20]. Extensive subsequent research delineated that oral microbes stimulate immune responses in barrier gingival tissues, which lead to paracrine signaling effects that impact osteoimmune processes in the proximal alveolar bone[17,56,83]. The current report innovatively utilized a gnotobiotic murine model colonized by a commensal gut bacterium to show that commensal gut microbe effects on systemic immunity influence alveolar bone homeostasis.

SFB was strategically chosen for the gnotobiotic murine model since the purpose was to associate mice with a commensal gut bacterium that does not colonize the oral cavity[69]. SFB was also selected based on the intent to utilize a commensal gut bacterium that modulates systemic immunity[31–38]. SFB regulation of systemic immunity has been shown to exacerbate inflammatory autoimmune conditions afflicting the central nervous system[84], lungs[85], and skeleton[42,43]. SFB driven T_H17/IL17A immune responses have been linked to changes in innate immune cells residing in the bone marrow[39,86], and SFB has been shown to expand marrow T_H17 cells[44,45]. Osteoimmunology studies have recently delineated that SFB immunomodulatory actions impact the development[44] and homeostasis[45] of osseous tissues at non-oral skeletal sites. Herein, we employed the SFB-monoassociated mouse model to show that commensal gut microbes have the capacity to regulate osteoimmune processes and skeletal homeostasis in the alveolar bone complex (Fig. 7).

SFB-monoassociated mice had a reduced skeletal phenotype in femur and alveolar bone. These findings show that commensal

gut microbe effects on skeletal tissue homeostasis are not limited to non-oral sites, but also extend to the alveolar bone complex. Study outcomes demonstrating that SFB colonized and induced immune response effects in intestinal mucosal tissues, but not oral mucogingival tissues, supports the notion that commensal gut microbe effects on alveolar bone are mediated through alterations in systemic immunity. The presence of SFB in the gut promoted an enhanced osteoclast phenotype in alveolar bone, which appears to be secondary to the increased fusion of pre-osteoclast/osteoclast cells. Candidate immune mediators supporting SFB pro-osteoclastic effects were identified, including upregulated circulating IL17A levels and increased T$_H$17 cells, activated CD4$^+$ T-cells, and *Tnf* in alveolar bone marrow.

Inflammatory changes in the gut[80] and the presence of SFB[45] increase IL17A and TNF expressing T-cells in bone marrow that drive osteoclast-mediated bone destruction at non-oral skeletal sites. IL17A and TNF signaling at osteoblastic cells upregulate the synthesis of pro-osteoclastic chemokines/cytokines that promote bone osteolysis[48–53]. Therefore, we speculated that SFB immunoregulatory actions supporting osteoclastogenesis in alveolar bone are mediated by IL17A and TNF paracrine signaling effects at osteoblastic cells. The osteoblast-osteoclast coupling assay discerned that osteoblast-derived CXCL1 and CCL2 support SFB actions promoting osteoclastogenesis. Supernatants from TNF-treated osteoblasts normalized osteoclast outcomes in GF and SPF mice, and this effect was dependent on CXCL1 and CCL2.

CXCL1 and CCL2 are IL17A and TNF responsive genes in osteoblasts[50,51,81,82]. Mechanical and ligand stimulation of osteoblastic cells induces CXCL1- and CCL2-mediated paracrine signaling that supports monocyte recruitment and osteoclast fusion/maturation[53,87–90]. The commensal gut microbiota has been shown to elicit *Ccl2* expression in BMMSCs[91], and we demonstrated that a commensal gut microbe promotes *Cxcl1* and *Ccl2* in BMMSCs. SFB-derived antigens and ligands stimulate immunity locally in the gut[38,47]. However, it is unclear whether these microbial signaling mediators pass into the bloodstream to signal to BMMSC/osteoblastic cells in the bone marrow environment.

The current report provides initial evidence that commensal gut microbes regulate osteoimmune processes and skeletal homeostasis in the alveolar bone complex. Indirect support for the concept that the gut microbiota influences alveolar bone homeostasis is provided by clinical oral manifestations of inflammatory bowel diseases. Inflammatory bowel conditions are linked to dysbiotic shifts in the indigenous gut microbiota[92,93]. Therefore, progressive alveolar bone loss observed in patients afflicted by inflammatory bowel diseases[94–96] may be related to changes in the gut microbiota. Further support for the concept that the gut microbiota affects alveolar bone homeostasis is lent by experimental periodontitis investigations. Probiotic bacteria strains naturally found in the gut have been shown to protect against periodontitis-driven alveolar bone loss[17,97–100]. Enteral administration of the probiotics via the oral route prevented alveolar bone destruction, which was associated with improved intestinal tissue morphology[97], reduced intestinal inflammation[98,99], and symbiotic effects on the gut microbiota[99]. Ongoing research is needed to discern how alterations in the commensal gut microbiota influence osteoimmune mechanisms regulating alveolar bone health and homeostasis.

DATA AVAILABILITY
The datasets used and/or analyzed during the current study are available from the corresponding author upon request.

REFERENCES
1. Microbial Ecology in States of Health and Disease: Workshop Summary. Forum on Microbial Health; Board on Global Health; Institute of Medicine., (National Academies Press (US): Washington (DC), 2014).
2. Belkaid, Y. & Harrison, O. J. Homeostatic immunity and the microbiota. *Immunity* **46**, 562–576 (2017).
3. Belkaid, Y. & Naik, S. Compartmentalized and systemic control of tissue immunity by commensals. *Nat. Immunol.* **14**, 646–653 (2013).
4. Ivanov, I. I. & Honda, K. Intestinal commensal microbes as immune modulators. *Cell Host Microbe* **12**, 496–508 (2012).
5. Thaiss, C. A., Zmora, N., Levy, M. & Elinav, E. The microbiome and innate immunity. *Nature* **535**, 65–74 (2016).
6. Brestoff, J. R. & Artis, D. Commensal bacteria at the interface of host metabolism and the immune system. *Nat. Immunol.* **14**, 676–684 (2013).
7. Blander, J. M., Longman, R. S., Iliev, I. D., Sonnenberg, G. F. & Artis, D. Regulation of inflammation by microbiota interactions with the host. *Nat. Immunol.* **18**, 851–860 (2017).
8. Sommer, F. & Backhed, F. The gut microbiota-masters of host development and physiology. *Nat. Rev. Microbiol.* **11**, 227–238 (2013).
9. Lackey, D. E. & Olefsky, J. M. Regulation of metabolism by the innate immune system. *Nat. Rev. Endocrinol.* **12**, 15–28 (2016).
10. Clemente, J. C., Ursell, L. K., Parfrey, L. W. & Knight, R. The impact of the gut microbiota on human health: an integrative view. *Cell* **148**, 1258–1270 (2012).
11. Sjogren, K. et al. The gut microbiota regulates bone mass in mice. *J. Bone Miner. Res.* **27**, 1357–1367 (2012).
12. Irie, K., Novince, C. M. & Darveau, R. P. Impact of the oral commensal flora on alveolar bone homeostasis. *J. Dent. Res.* **93**, 801–806 (2014).
13. Novince, C. M. et al. Commensal gut microbiota immunomodulatory actions in bone marrow and liver have catabolic effects on skeletal homeostasis in health. *Sci. Rep.* **7**, 5747 (2017).
14. Li, J. Y. et al. Sex steroid deficiency-associated bone loss is microbiota dependent and prevented by probiotics. *J. Clin. Investig.* **126**, 2049–2063 (2016).
15. Walsh, M. C., Takegahara, N., Kim, H. & Choi, Y. Updating osteoimmunology: regulation of bone cells by innate and adaptive immunity. *Nat. Rev. Rheumatol.* **14**, 146–156 (2018).
16. Novince, C. M. & Kirkwood, K. L. Alveolar bone homeostasis in health and disease. In: J. P. Bilezikian (ed). Primer on the Metabolic Bone Diseases and Disorders of Mineral Metabolism. 933–940 (Wiley-Blackwell: Ames, Iowa, 2019).
17. Hathaway-Schrader, J. D. & Novince, C. M. Maintaining homeostatic control of periodontal bone tissue. *Periodontology 2000* **86**, 157–187 (2021).
18. Garant, P. R. Light and electron microscopic observations of osteoclastic alveolar bone resorption in rats monoinfected with Actinomyces naeslundii. *J. Periodontol.* **47**, 717–723 (1976).
19. Behling, U. H., Sallay, C., Sanavi, F., Pham, P. H. & Nowotny, A. Humoral immunity and reduced periodontal bone loss in Eikenella corrodens-monoassociated rats. *Infect. Immun.* **33**, 801–805 (1981).
20. Burckhardt, J. J., Gaegauf-Zollinger, R., Schmid, R. & Guggenheim, B. Alveolar bone loss in rats after immunization with Actinomyces viscosus. *Infect. Immun.* **31**, 971–977 (1981).
21. Klaasen, H. L., Koopman, J. P., Poelma, F. G. & Beynen, A. C. Intestinal, segmented, filamentous bacteria. *FEMS Microbiol. Rev.* **8**, 165–180 (1992).
22. Klaasen, H. L. et al. Intestinal, segmented, filamentous bacteria in a wide range of vertebrate species. *Lab. Anim.* **27**, 141–150 (1993).
23. Snel, J. et al. Comparison of 16S rRNA sequences of segmented filamentous bacteria isolated from mice, rats, and chickens and proposal of "Candidatus Arthromitus". *Int. J. Syst. Bacteriol.* **45**, 780–782 (1995).
24. Yin, Y. et al. Comparative analysis of the distribution of segmented filamentous bacteria in humans, mice and chickens. *ISME J.* **7**, 615–621 (2013).
25. Chen, B. et al. Presence of segmented filamentous bacteria in human children and its potential role in the modulation of human gut immunity. *Front. Microbiol.* **9**, 1403 (2018).
26. Chen, H. et al. Distribution and strain diversity of immunoregulating segmented filamentous bacteria in human intestinal lavage samples. *Microb. Ecol.* **79**, 1021–1033 (2020).
27. Klaasen, H. L. K., J., P. & Beynen, A. C. Effects of age, strain and social hierarchy on colonization of autochthonous, segmented, filamentous bacteria in the ileum of mice. *Microecology Ther.* **20**, 17–20 (1990b).
28. Snel, J. et al. Interactions between gut-associated lymphoid tissue and colonization levels of indigenous, segmented, filamentous bacteria in the small intestine of mice. *Can. J. Microbiol.* **44**, 1177–1182 (1998).
29. Talham, G. L., Jiang, H. Q., Bos, N. A. & Cebra, J. J. Segmented filamentous bacteria are potent stimuli of a physiologically normal state of the murine gut mucosal immune system. *Infect. Immun.* **67**, 1992–2000 (1999).
30. Jiang, H. Q., Bos, N. A. & Cebra, J. J. Timing, localization, and persistence of colonization by segmented filamentous bacteria in the neonatal mouse gut depend on immune status of mothers and pups. *Infect. Immun.* **69**, 3611–3617 (2001).
31. Ivanov, I. I. et al. Induction of intestinal Th17 cells by segmented filamentous bacteria. *Cell* **139**, 485–498 (2009).

32. Gaboriau-Routhiau, V. et al. The key role of segmented filamentous bacteria in the coordinated maturation of gut helper T cell responses. *Immunity* **31**, 677–689 (2009).

33. Goto, Y. et al. Segmented filamentous bacteria antigens presented by intestinal dendritic cells drive mucosal Th17 cell differentiation. *Immunity* **40**, 594–607 (2014).

34. Lecuyer, E. et al. Segmented filamentous bacterium uses secondary and tertiary lymphoid tissues to induce gut IgA and specific T helper 17 cell responses. *Immunity* **40**, 608–620 (2014).

35. Atarashi, K. et al. Th17 cell induction by adhesion of microbes to intestinal epithelial cells. *Cell* **163**, 367–380 (2015).

36. Panea, C. et al. Intestinal monocyte-derived macrophages control commensal-specific Th17 responses. *Cell Rep.* **12**, 1314–1324 (2015).

37. Flannigan, K. L. et al. IL-17A-mediated neutrophil recruitment limits expansion of segmented filamentous bacteria. *Mucosal. Immunol.* **10**, 673–684 (2017).

38. Ladinsky, M. S., et al. Endocytosis of commensal antigens by intestinal epithelial cells regulates mucosal T cell homeostasis. *Science* **363**, 1–10 (2019).

39. Burgess, S. L. et al. Bone marrow dendritic cells from mice with an altered microbiota provide interleukin 17A-dependent protection against Entamoeba histolytica colitis. *MBio* **5**, e01817 (2014).

40. Shi, Z. et al. Segmented filamentous bacteria prevent and cure rotavirus infection. *Cell* **179**, 644–658 (2019). e613.

41. Gauguet, S. et al. Intestinal microbiota of mice influences resistance to Staphylococcus aureus pneumonia. *Infect. Immun.* **83**, 4003–4014 (2015).

42. Wu, H. J. et al. Gut-residing segmented filamentous bacteria drive autoimmune arthritis via T helper 17 cells. *Immunity* **32**, 815–827 (2010).

43. Chappert, P., Bouladoux, N., Naik, S. & Schwartz, R. H. Specific gut commensal flora locally alters T cell tuning to endogenous ligands. *Immunity* **38**, 1198–1210 (2013).

44. Hathaway-Schrader, J. D. et al. Specific commensal bacterium critically regulates gut microbiota osteoimmunomodulatory actions during normal postpubertal skeletal growth and maturation. *JBMR Plus* **4**, e10338 (2020).

45. Yu, M. et al. PTH induces bone loss via microbial-dependent expansion of intestinal TNF(+) T cells and Th17 cells. *Nat. Commun.* **11**, 468 (2020).

46. Schnupf, P. et al. Growth and host interaction of mouse segmented filamentous bacteria in vitro. *Nature* **520**, 99–103 (2015).

47. Wang, Y. et al. Induction of intestinal Th17 cells by flagellins from segmented filamentous bacteria. *Front. Immunol.* **10**, 2750 (2019).

48. Thomson, B. M., Mundy, G. R. & Chambers, T. J. Tumor necrosis factors alpha and beta induce osteoblastic cells to stimulate osteoclastic bone resorption. *J. Immunol.* **138**, 775–779 (1987).

49. Kotake, S. et al. IL-17 in synovial fluids from patients with rheumatoid arthritis is a potent stimulator of osteoclastogenesis. *J. Clin. Investig.* **103**, 1345–1352 (1999).

50. Ruddy, M. J., Shen, F., Smith, J. B., Sharma, A. & Gaffen, S. L. Interleukin-17 regulates expression of the CXC chemokine LIX/CXCL5 in osteoblasts: implications for inflammation and neutrophil recruitment. *J. Leukoc. Biol.* **76**, 135–144 (2004).

51. Shen, F., Ruddy, M. J., Plamondon, P. & Gaffen, S. L. Cytokines link osteoblasts and inflammation: microarray analysis of interleukin-17- and TNF-alpha-induced genes in bone cells. *J. Leukoc. Biol.* **77**, 388–399 (2005).

52. Souza, P. P. & Lerner, U. H. The role of cytokines in inflammatory bone loss. *Immunol. Investig.* **42**, 555–622 (2013).

53. Brylka, L. J. & Schinke, T. Chemokines in physiological and pathological bone remodeling. *Front. Immunol.* **10**, 2182 (2019).

54. Bouxsein, M. L. et al. Guidelines for assessment of bone microstructure in rodents using micro-computed tomography. *J. Bone Miner. Res.* **25**, 1468–1486 (2010).

55. Hathaway-Schrader, J. D. et al. Antibiotic perturbation of gut microbiota dysregulates osteoimmune cross talk in postpubertal skeletal development. *Am. J. Pathol.* **189**, 370–390 (2019).

56. Kinane, D. F., Stathopoulou, P. G. & Papapanou, P. N. Periodontal diseases. *Nat. Rev. Dis. Primers* **3**, 17038 (2017).

57. Dempster, D. W. et al. Standardized nomenclature, symbols, and units for bone histomorphometry: a 2012 update of the report of the ASBMR Histomorphometry Nomenclature Committee. *J. Bone Miner. Res.* **28**, 2–17 (2013).

58. Schnupf, P., Gaboriau-Routhiau, V. & Cerf-Bensussan, N. Host interactions with Segmented Filamentous Bacteria: an unusual trade-off that drives the post-natal maturation of the gut immune system. *Semin. Immunol.* **25**, 342–351 (2013).

59. Farkas, A. M. et al. Induction of Th17 cells by segmented filamentous bacteria in the murine intestine. *J. Immunol. Methods* **421**, 104–111 (2015).

60. Bacchetti De Gregoris, T., Aldred, N., Clare, A. S. & Burgess, J. G. Improvement of phylum- and class-specific primers for real-time PCR quantification of bacterial taxa. *J. Microbiol. Methods* **86**, 351–356 (2011).

61. Gaboriau-Routhiau, V., Lecuyer, E. & Cerf-Bensussan, N. Role of microbiota in postnatal maturation of intestinal T-cell responses. *Curr. Opin. Gastroenterol.* **27**, 502–508 (2011).

62. Livak, K. J. & Schmittgen, T. D. Analysis of relative gene expression data using real-time quantitative PCR and the 2(-Delta Delta C(T)) Method. *Methods* **25**, 402–408 (2001).

63. Schmittgen, T. D. & Livak, K. J. Analyzing real-time PCR data by the comparative C(T) method. *Nat. Protoc.* **3**, 1101–1108 (2008).

64. Umesaki, Y., Okada, Y., Matsumoto, S., Imaoka, A. & Setoyama, H. Segmented filamentous bacteria are indigenous intestinal bacteria that activate intraepithelial lymphocytes and induce MHC class II molecules and fucosyl asialo GM1 glycolipids on the small intestinal epithelial cells in the ex-germ-free mouse. *Microbiol. Immunol.* **39**, 555–562 (1995).

65. Page, R. C. & Schroeder, H. E. Periodontitis in Man and Other Animals: a Comparative Review. (Karger: New York, 1982).

66. Tucker, A. & Sharpe, P. The cutting-edge of mammalian development; how the embryo makes teeth. *Nat. Rev. Genet.* **5**, 499–508 (2004).

67. Treuting, P. M., Morton, T. H. & Vogel, P. Oral Cavity and Teeth. In: Piper M. Treuting, Suzanne M. Dintzis, & Kathleen S. Montine (eds). Comparative Anatomy and Histology (Second Edition) 115–133 (Academic Press: San Diego, 2018).

68. Cho, M. I. & Garant, P. R. Development and general structure of the periodontium. *Periodontol 2000* **24**, 9–27 (2000).

69. Dutzan, N. et al. On-going mechanical damage from mastication drives homeostatic Th17 cell responses at the oral barrier. *Immunity* **46**, 133–147 (2017).

70. Weitzmann, M. N. & Ofotokun, I. Physiological and pathophysiological bone turnover—role of the immune system. *Nat. Rev. Endocrinol.* **12**, 518–532 (2016).

71. Redlich, K. & Smolen, J. S. Inflammatory bone loss: pathogenesis and therapeutic intervention. *Nat. Rev. Drug Discov.* **11**, 234–250 (2012).

72. Monasterio, G. et al. Capsular-defective Porphyromonas gingivalis mutant strains induce less alveolar bone resorption than W50 wild-type strain due to a decreased Th1/Th17 immune response and less osteoclast activity. *J. Periodontol.* **90**, 522–534 (2019).

73. Dutzan, N., *et al.* A dysbiotic microbiome triggers TH17 cells to mediate oral mucosal immunopathology in mice and humans. *Sci. Transl. Med.* **10**, 1–12 (2018).

74. Tsukasaki, M. et al. Host defense against oral microbiota by bone-damaging T cells. *Nat. Commun.* **9**, 701 (2018).

75. Martin, T. J. & Sims, N. A. RANKL/OPG; critical role in bone physiology. *Rev. Endocr. Metab. Disord.* **16**, 131–139 (2015).

76. Boyce, B. F. & Xing, L. Functions of RANKL/RANK/OPG in bone modeling and remodeling. *Arch. Biochem. Biophys.* **473**, 139–146 (2008).

77. Kukita, T. et al. RANKL-induced DC-STAMP is essential for osteoclastogenesis. *J. Exp. Med.* **200**, 941–946 (2004).

78. Yagi, M. et al. DC-STAMP is essential for cell-cell fusion in osteoclasts and foreign body giant cells. *J. Exp. Med.* **202**, 345–351 (2005).

79. Mbalaviele, G., Novack, D. V., Schett, G. & Teitelbaum, S. L. Inflammatory osteolysis: a conspiracy against bone. *J. Clin. Investig.* **127**, 2030–2039 (2017).

80. Ciucci, T. et al. Bone marrow Th17 TNFalpha cells induce osteoclast differentiation, and link bone destruction to IBD. *Gut* **64**, 1072–1081 (2015).

81. Graves, D. T., Jiang, Y. & Valente, A. J. The expression of monocyte chemoattractant protein-1 and other chemokines by osteoblasts. *Front. Biosci.* **4**, D571–D580 (1999).

82. Di Benedetto, G. et al. Redundant modulatory effects of proinflammatory cytokines in human osteoblastic cells in vitro. *Clin. Exp. Rheumatol.* **36**, 959–969 (2018).

83. Curtis, M. A., Zenobia, C. & Darveau, R. P. The relationship of the oral microbiotia to periodontal health and disease. *Cell Host Microbe* **10**, 302–306 (2011).

84. Lee, Y. K., Menezes, J. S., Umesaki, Y. & Mazmanian, S. K. Proinflammatory T-cell responses to gut microbiota promote experimental autoimmune encephalomyelitis. *Proc. Natl Acad. Sci USA* **108**, 4615–4622 (2011). Suppl 1.

85. Bradley, C. P. et al. Segmented filamentous bacteria provoke lung autoimmunity by inducing gut-lung axis Th17 cells expressing dual TCRs. *Cell Host Microbe* **22**, 697–704 (2017). e694.

86. Xu, C., Lee, S. K., Zhang, D. & Frenette, P. S. The gut microbiome regulates psychological-stress-induced inflammation. *Immunity* **53**, 417–428 (2020).

87. Rahimi, P. et al. Monocyte chemoattractant protein-1 expression and monocyte recruitment in osseous inflammation in the mouse. *Endocrinology* **136**, 2752–2759 (1995).

88. Li, X. et al. Parathyroid hormone stimulates osteoblastic expression of MCP-1 to recruit and increase the fusion of pre/osteoclasts. *J. Biol. Chem.* **282**, 33098–33106 (2007).

89. Cambré, I. et al. Mechanical strain determines the site-specific localization of inflammation and tissue damage in arthritis. *Nat Commun* **9**, 4613 (2018).

90. Onan, D. et al. The chemokine Cxcl1 is a novel target gene of parathyroid hormone (PTH)/PTH-related protein in committed osteoblasts. *Endocrinology* **150**, 2244–2253 (2009).

91. Xiao, E. et al. Microbiota regulates bone marrow mesenchymal stem cell lineage differentiation and immunomodulation. *Stem Cell Res. Ther.* **8**, 213 (2017).

92. Sommer, F., Anderson, J. M., Bharti, R., Raes, J. & Rosenstiel, P. The resilience of the intestinal microbiota influences health and disease. *Nat. Rev. Microbiol.* **15**, 630–638 (2017).

93. Nishida, A. et al. Gut microbiota in the pathogenesis of inflammatory bowel disease. *Clin. J. Gastroenterol.* **11**, 1–10 (2018).

94. Lamster, I., Sonis, S., Hannigan, A. & Kolodkin, A. An association between Crohn's disease, periodontal disease and enhanced neutrophil function. *J. Periodontol.* **49**, 475–479 (1978).

95. Ozmeric, N., Bissada, N. & da Silva, A. P. B. The association between inflammatory bowel disease and periodontal conditions: is there a common bacterial etiology? *J. Int. Acad. Periodontol.* **20**, 40–51 (2018).

96. She, Y. Y. et al. Periodontitis and inflammatory bowel disease: a meta-analysis. *BMC Oral Health* **20**, 67 (2020).

97. Messora, M. R. et al. Probiotic therapy reduces periodontal tissue destruction and improves the intestinal morphology in rats with ligature-induced periodontitis. *J. Periodontol.* **84**, 1818–1826 (2013).

98. Kobayashi, R. et al. Oral administration of Lactobacillus gasseri SBT2055 is effective in preventing Porphyromonas gingivalis-accelerated periodontal disease. *Sci. Rep.* **7**, 545 (2017).

99. Gatej, S. M. et al. Probiotic Lactobacillus Rhamnosus GG protects against P. Gingivalis And F. Nucleatum gut dysbiosis. *J. Int. Acad. Periodontol.* **22**, 18–27 (2020).

100. Gatej, S., Gully, N., Gibson, R. & Bartold, P. M. Probiotics and periodontitis—a literature review. *J. Int. Acad. Periodontol.* **19**, 42–50 (2017).

ACKNOWLEDGEMENTS

FUNDING STATEMENT

AUTHOR CONTRIBUTIONS

Designed research: J.D.H., C.W., C.M.N.; Performed research: J.D.H., M.D.C., J.E.G., A.J.W., B.A.S., J.I.A., C.W., C.M.N.; Analyzed data: J.D.H., M.D.C., J.E.G., A.J.W., B.A.S., B.L., C.M.N.; Drafting manuscript: J.D.H., C.M.N.; Revised manuscript: J.D.H., M.D.C., J.E.G., A.J.W., B.A.S., J.I.A., C.W., B.L., C.M.N. All authors gave their final approval and agreed to be accountable for all aspects of the work.

COMPETING INTERESTS

The authors declare no competing interests.

ADDITIONAL INFORMATION

Supplementary information The online version contains supplementary material available at https://doi.org/10.1038/s41374-021-00697-0.

Correspondence and requests for materials should be addressed to Chad M. Novince.

Reprints and permission information is available at http://www.nature.com/reprints

Publisher's note Springer Nature remains neutral with regard to jurisdictional claims in published maps and institutional affiliations.